Journal of Molecular Structure 1044 (2013) 21–25

Contents lists available at SciVerse ScienceDirect

Journal of Molecular Structure

journal homepage: www.elsevier.com/locate/molstruc

# High resolution spectroscopy of several rovibronically excited bands of 5-cyanoindole – The effect of vibrational averaging

Christian Brand, Beatrice Happe, Olivia Oeltermann, Martin Wilke, Michael Schmitt *

*Heinrich-Heine-Universität, Institut für Physikalische Chemie I, D-40225 Düsseldorf, Germany*

ARTICLE INFO

*Article history:*
Available online 5 December 2012

*Keywords:*
Electronic spectroscopy
Rotational resolution
5-Cyanoindole
Vibronic coupling
Vibrational averaging

ABSTRACT

The rovibronic spectra of two bands of 5-cyanoindole at 348 and 884 $cm^{-1}$ have been measured and analyzed using a rigid rotor Hamiltonian. A vibrational assignment could be given on the basis of an anharmonic analysis of the vibrational spectrum of 5-cyanoindole making use of the information of the vibrationally averaged rotational constants. Strong vibronic mixing to a higher lying electronically excited state has been found.



## 1. Introduction

The photophysics and photochemistry of indole and substituted indoles is governed by the existence of two electronically excited singlet states, which are labeled $^1L_a$ and $^1L_b$ following the nomenclature of Platt for catacondensed aromatics [1]. Depending on the substituent the energy difference between these two states differs largely, in some cases even their energetic order is reversed. Vibronic spectroscopy with rotational resolution provides an elegant approach to the nature of the excited states via determination of the transition dipole moment directions.

For indole it is generally accepted now, that the lowest electronically excited singlet state of indole is a state with $L_b$ character, followed by an $L_a$ like state, approximately 1400 $cm^{-1}$ higher in energy [2–7]. This has been shown by quantum chemical calculations [2,5] from the theory side and by two-photon-induced fluorescence anisotropy measurements [3], two-photon excitation spectroscopy [4], linear dichroism measurements on partially oriented indole in stretched polyethylene films [8], and by rotationally resolved spectroscopy of vibronic bands of indole [6,7].

The introduction of substituents in different positions of the chromophore may change this energetic separation of the two states and sometimes even reverse them. For 5-methoxyindole the $^1L_a$ state is predicted to lie more than 4000 $cm^{-1}$ above the $^1L_b$ state, one of the largest gaps in the indole row [9]. For isolated tetrahydrocarbazole, on the other hand, it could be shown that the lowest excited singlet state is the $^1L_a$ state [10], while for 2,3-dimethylindole the energy order critically depends on the local surrounding of the chromophore. Even a small perturbation like an argon matrix as local surrounding shifts the $^1L_a$ state below the $^1L_b$, with a reversed order in gas phase [11–13]. In gas phase the spectral position and lifetime of the electronic origin of 5CI were determined by Huang and Sulkes using time-correlated single photon counting for $S_1$ levels in supersonic free jet expansions [14]. The rotationally resolved spectrum of the electronic origin was measured and analyzed by Oeltermann et al. [15].

In the present publication we show, how the information of vibrationally averaged rotational constants can be utilized for a straightforward assignment of rovibronic spectra.

## 2. Techniques

### 2.1. Experimental procedures

5CI (⩾98%) was purchased from Activate Scientific and used without further purification. The experimental set up for the rotationally resolved laser induced fluorescence is described in detail elsewhere [16]. In brief, the laser system consists of a single frequency ring dye laser (Sirah Matisse DS) operated with Rhodamine 6G, pumped with 8 W of the 514 nm line of a $Ar^+$-ion laser (Coherent, Sabre 15 DBW). The dye laser output was coupled into an external folded ring cavity (Spectra Physics Wavetrain) for second harmonic generation. The resulting output power was constant at about 30 mW during the experiment. The molecular beam was formed by co-expanding 5CI, heated to 190 °C, and 400 mbar of argon through a 200 μm nozzle into the vacuum chamber. The molecular beam machine consists of three differentially pumped vacuum chambers that are linearly connected by skimmers (1 mm and 3 mm, respectively) in order to reduce the

* Corresponding author.
*E-mail address:* mschmitt@uni-duesseldorf.de (M. Schmitt).

0022-2860/$ - see front matter © 2012 Elsevier B.V. All rights reserved.
http://dx.doi.org/10.1016/j.molstruc.2012.11.049

Doppler width. The resulting resolution is 18 MHz (FWHM) in this set-up. In the third chamber, 360 mm downstream of the nozzle, the molecular beam crosses the laser beam at a right angle. The imaging optics setup consists of a concave mirror and two plano-convex lenses to focus the resulting fluorescence onto a photomultiplier tube, which is mounted perpendicularly to the plane defined by the laser and molecular beam. The signal output was then discriminated and digitized by a photon counter and transmitted to a PC for data recording and processing. The relative frequency was determined with a *quasi* confocal Fabry–Perot interferometer. The absolute frequency was obtained by comparing the recorded spectrum to the tabulated lines in the iodine absorption spectrum [17].

### 2.2. Computational methods

#### 2.2.1. Quantum chemical calculations

Structure optimizations were performed employing Dunning's correlation consistent polarized valence triple zeta (cc-pVTZ) from the TURBOMOLE library [18,19]. The equilibrium geometries of the electronic ground and the lowest excited singlet states were optimized using the approximate coupled cluster singles and doubles model (CC2) employing the resolution-of-the-identity approximation (RI) [20–22] including spin-component scaling (SCS) modifications to CC2 [23]. All CC2 calculations were carried out utilizing the TURBOMOLE package, version 6.1 [24]. Vibrational frequencies and zero-point corrections to the adiabatic excitation energies have been obtained from numerical second derivatives using the NumForce script [24].

An anharmonic analysis of the vibrational spectrum allows for the determination of vibrational averaging effects due to the individual vibrational motion [25]. Such an anharmonic analysis is implemented in the Gaussian program package [26]. The procedure for the calculation of cubic and of some of the quartic force constants utilizes third derivatives of the potential energy with respect to the normal coordinates. They are calculated for the electronic ground state using numerical derivatives of analytical second derivatives of the MP2 energies using the 6-31G(d,p) basis set. We tried to calculate the same quantities for the excited state vibrational levels using CC2 theory. Since for CC2, only numerical second derivatives are available, numerical instabilities in the calculation of the third derivatives were too large to make the method of any use.

#### 2.2.2. Fits of the rovibronic spectra using evolutionary algorithms

The optimization algorithm employed in the fit of molecular constants to the rotationally resolved electronic spectra is an evolutionary strategy adapting mutations *via* a covariance matrix adaptation (CMA-ES) mechanism. This algorithm was developed by Ostenmeier et al. [27], and Hansen and Ostenmeier [28]. It belongs, like other search algorithms that are also used in our group (genetic algorithms (GAs) [29] and evolutionary strategy employing second generation of derandomized evolutionary strategies (ES-DR2) [30]), to the group of global optimizers that were inspired by natural evolution. For a detailed description of this evolutionary strategy we refer to Refs. [9,29].

## 3. Results and discussion

### 3.1. High resolution spectra of several vibronic bands of 5-cyanoindole

Fig. 1 shows the rotationally resolved spectrum of the electronic origin of 5CI at 33874 $cm^{-1}$, taken from the publication by Oeltermann et al. [15]. The authors simulated the experimental spectrum with a rigid rotor Hamiltonian and almost pure *a*-type selection rules (the transition dipole moment (TDM) angle $\theta$ is determined to be 3°, equivalent to less than 1% *b*-type for the spectrum). In the course of the present study we refitted this spectra using the CMA-ES strategy, and the values determined for all molecular parameter are well within the boundaries published previously. To facilitate the comparison for the vibrational bands, these values are given in Table 1. The enlarged portion detail of the spectrum shows the excellent agreement between experiment and simulation using the parameters from the best fit employing the CMA-ES strategy. The fit of the line shapes to Voigt profiles using a Gaussian (Doppler) contribution of 18 MHz yielded a Lorentzian contribution of 13 ± 1 MHz to the total line width equivalent to an excited state life time of 12 ± 1 ns, in fair agreement with the value from time-resolved spectroscopy of 16.9 ns by Huang and Sulkes [14].

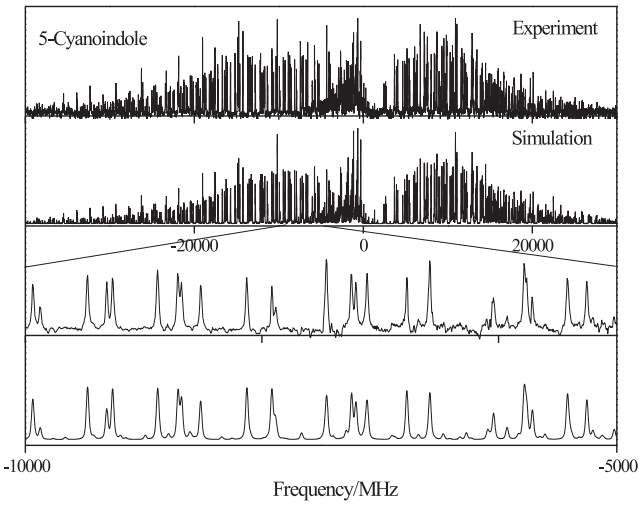


**Fig. 1.** Rotationally resolved electronic spectrum of the electronic origin of 5-cyanoindole.

The rovibronic spectra of the 0, 0 + 349 and 0, 0 + 884 $cm^{-1}$ bands along with the simulations using the best fit parameters, given in Table 1 are shown in Figs. 2 and 3. In the fit of the molecular parameters to the experimental spectra, we have set the rotational constants of the ground state to the values determined from the fit of the electronic origin. This is justified by the fact, that the signal/noise ratio is nearly two orders of magnitude better for the origin band. Both excited vibronic bands exhibit a considerably larger *b*-type character than the origin band, with TDM angles of 33° and 23°. The lifetime of the 349 $cm^{-1}$ band increases to 18 ± 2 ns compared to 12 ± 1 ns for both the origin and the 884 $cm^{-1}$ band.

### 3.2. Computational results

#### 3.2.1. Structure and vibrational averaging

Commonly, the vibrationally averaged inertial parameters, which are obtained from the experiment are compared to equilibrium values at the potential energy minimum, obtained from quantum chemical calculations. Table 1 collects the structural data; i.e., the rotational constants (*A*,*B*, and *C*) in the electronic ground (double prime) and excited (single prime) states, their changes upon electronic excitation ($\Delta A$,$\Delta B$, and $\Delta C$), and the respective inertial defects.[1]

[1] The inertial defect is a measure for the non-planarity of a molecule in a given electronic state, and is defined as: $\Delta I = I_C - I_A - I_B$. For a planar molecule it is close to zero with out-of-plane vibrations generally causing a negative contribution to the inertial defect, and in-plane vibrations often having a small positive contribution [31].

**Table 1**
Molecular constants of the electronic origin and of two vibronically excited bands of 5-cyanoindole obtained from the ES-DR2 fits of the experimental spectra. Changes of the rotational constants are defined as: $\Delta B_g = B'_g - B''_g$, with $B_g$ as rotational constants with respect to the inertial axes $g = a, b, c$ with primed quantities, defining the excited state and double primed the electronic ground state, respectively. The superscript *e* refers to the rotational constants at the equilibrium geometry, the superscript 0 to the zero-point vibrational averaged inertial parameters.

| | Experiment | | | Theory | | |
|---|---|---|---|---|---|---|
| | Origin[a] | +349 | +884 | SCS-CC2[c] | MP2($B^e$)[d] | MP2($B^0$)[d] |
| $A''$ (MHz) | 3370.36(16) | 3370.36[b] | 3370.36[b] | 3364 | 3364 | 3346 |
| $B''$ (MHz) | 738.00(2) | 738.00[b] | 738.00[b] | 734 | 734 | 731 |
| $C''$ (MHz) | 605.53(1) | 605.53[b] | 605.53[b] | 602 | 603 | 600 |
| $\Delta I''$ (amu Å$^2$) | −0.1385 | −0.1385 | −0.1385 | 0.0 | 0.0 | −0.15 |
| $A'$ (MHz) | 3299.9(16) | 3300.3(2) | 3295.8(2) | 3281 | – | – |
| $B'$ (MHz) | 730.32(3) | 730.33(2) | 730.37(1) | 725 | – | – |
| $C'$ (MHz) | 598.16(2) | 598.53(1) | 598.67(1) | 594 | – | – |
| $\Delta I'$ (amu Å$^2$) | −0.2582 | −0.7575 | −1.1246 | 0.0 | – | – |
| $\Delta A$ (MHz) | −70.46(1) | −70.10(1) | −74.64(1) | −83 | – | – |
| $\Delta B$ (MHz) | −7.68(1) | −7.67(1) | −7.63(1) | −9 | – | – |
| $\Delta C$ (MHz) | −7.37(1) | −7.40(1) | −7.26(1) | −6 | – | – |
| $\theta$ (°) | 3(3) | 32(1) | 22(1) | 9.4 | – | – |
| $\nu_0$ (cm$^{-1}$) | 33874.32 | 34223.08 | 34757.89 | 34811 | – | – |
| $\Delta$*Lorentz* (MHz) | 13(1) | 9(1) | 13(1) | – | – | – |

[a] From Ref. [15].
[b] Held fixed at the values of the electronic origin.
[c] Using the cc-pVTZ basis set.
[d] Using the 6-31G(d,p) basis set.

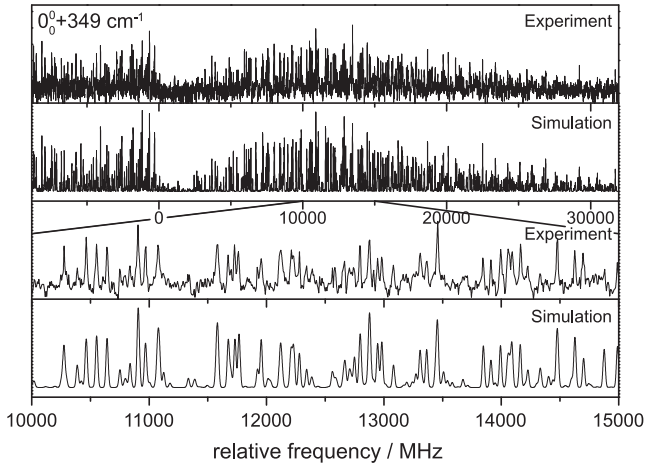


**Fig. 2.** Rotationally resolved electronic spectrum of the vibronic band at 0, 0 + 348 cm$^{-1}$.

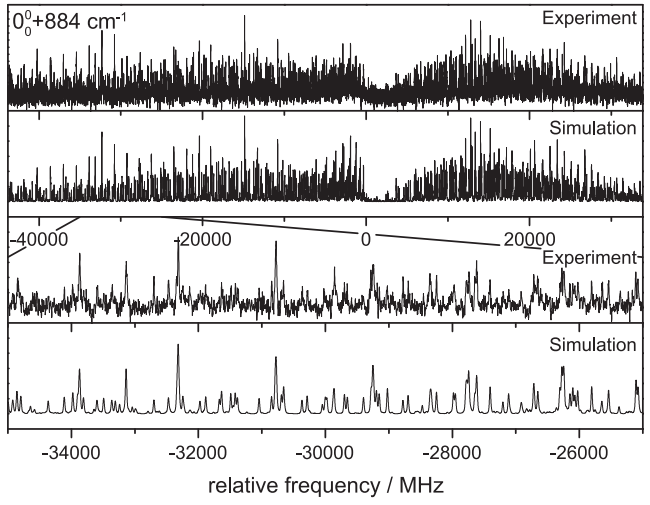


**Fig. 3.** Rotationally resolved electronic spectrum of the vibronic band at 0, 0 + 884 cm$^{-1}$.

The equilibrium structures of the ground and electronically excited states, optimized at the SCS-CC2 and MP2 levels of theory, are planar without imposing symmetry constraints during the optimization. Their *ab initio* calculated inertial defects are therefore exactly zero. The experimental values contain vibrational corrections from the vibrational averaging of the ground and excited state structures. The difference of the experimental and the calculated $\Delta I$ values gives 1% as first order approximation to the amount of vibrational averaging contained in the experimental rotational constants.

For the electronic ground state the zero-point vibrationally averaged rotational constants are compiled in Table 1. While the inertial defect calculated using the equilibrium inertial parameters is exactly zero as expected for a planar structure, it amounts to −0.15 amu Å$^2$ for the vibrationally averaged rotational constants, very close to the experimental value of −0.1385 amu Å$^2$. We thus conclude, that vibrational averaging of the rotational constants is sufficiently well described by the quadratic, cubic and some of the quartic force constants as included in this study. The deviations between the experimental rotational constants and the vibrationally zero-point averaged calculated values amount to less than 1%, thus confirming our first approximation. The complete list of anharmonic and harmonic frequencies, vibrationally averaged rotational constants and inertial defects is given in the online supplementary material (Table S4).

**Table 2**
Inertial defects of the excited vibronic states $\Delta I'$, vibrational contributions to the rotational constants of the excited vibronic states $\Delta A'_{vib}$, $\Delta B'_{vib}$, $\Delta C'_{vib}$ (defined as $\Delta X_{vib}(Q_i) = X(Q_i) - X(Q_0)$). Experimental values are extracted from the parameters in Table 1, calculated values are from an anharmonic analysis of the electronic ground state at the MP2/6-31G(d,p) level of theory; see text for details.

| Vibration | $0_0^0$ | | $43_0^1$ | | $28_0^1$ | |
|---|---|---|---|---|---|---|
| | Exp. | Calc. | Exp. | Calc. | Exp. | Calc. |
| $\nu$ (cm$^{-1}$) | – | – | 349 | 338 | 884 | 869 |
| $\Delta I'$ (amu Å$^2$) | −0.14 | −0.15 | −0.76 | −0.63 | −1.12 | −0.38 |
| $\Delta A'_{vib}$ (MHz) | – | – | +0.4 | −0.6 | −4.1 | −2.2 |
| $\Delta B'_{vib}$ (MHz) | – | – | ±0.0 | ±0.0 | +0.1 | ±0.0 |
| $\Delta C'_{vib}$ (MHz) | – | – | +0.4 | +0.3 | +0.5 | ±0.0 |

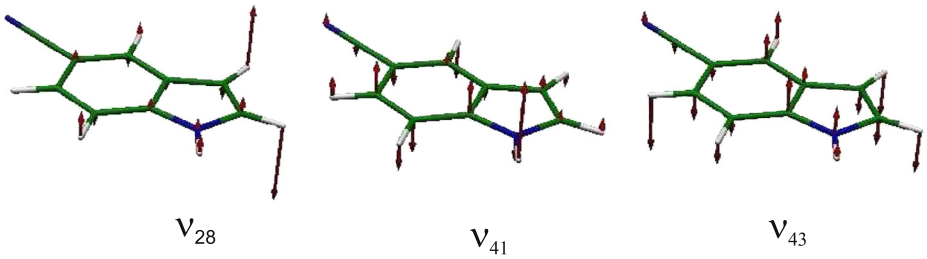


**Fig. 4.** Vibrational modes 28, 41, and 43.

An analysis of the electronically excited state vibrations can be performed under the assumption, that the directions and amplitudes of the vibrational displacement vectors are similar in the ground and the electronically excited states. The change of the rotational constants upon vibronic excitation can then be calculated from the sum of the zero-point averaged changes due to pure electronic excitation and to changes due to the individual vibrational excitation. The former are experimentally obtained from the changes of the rotational constants of the vibrationless origin (cf. Table 1), the latter from the vibrational anharmonic analysis, compiled in Table 2.

The assignment of the 349 $cm^{-1}$ band to vibration 43 (cf. Table S4) and of the 884 $cm^{-1}$ band to vibration 28 has been made on the basis of three independent pieces of information. The calculated (anharmonic) vibrational frequencies are utilized in order to narrow down the range of possible modes. Then the vibrationally induced changes of the inertial defects and rotational constants are compared to the experimental values. As these changes are most pronounced for the $A'$ rotational constant, we attribute the main influence to it. In the case of the 349 $cm^{-1}$ band an assignment which is only based on vibrational frequencies could also be made to mode 39 ($\nu_{anharm}$ = 384 $cm^{-1}$) or mode 42 ($\nu_{anharm}$ = 326 $cm^{-1}$) (cf. Table S4). Judging from a comparison of the inertial defect, however, mode 39 has to be excluded as $\Delta I'$ increases for this mode, quite in contrast to the experimental finding. Moreover, this vibration has a relatively large anharmonic correction to the $A'$ rotational constant of +4.6 MHz, which stands in further contradiction to the experimental finding of +0.4 MHz. This slight impact of the vibration on $A'$ is only mirrored by mode 43 ($\Delta A'_{vib} = -0.6$ MHz). For mode 42, the resulting inertial defect matches the experiment, but $\Delta A'_{vib}$ decreases too much (−4.5 MHz).

Mode 28 at 884 $cm^{-1}$ is first assigned on the basis of the anharmonic frequency (869 $cm^{-1}$). Also, an assignment to mode 24 (902 $cm^{-1}$) or 29 (855 $cm^{-1}$) based on the frequency information alone would be possible, but the quite large negative inertial defect of the mode contradicts at least an assignment to mode 24. The preference to mode 28 is based on the significant decrease of the $A'$ rotational constant which is not reproduced by mode 29.

The displacement vectors of the modes 28 and 43, which are assigned as being responsible for the 349 $cm^{-1}$ and the 869 $cm^{-1}$ bands are shown in Fig. 4 together with mode 41. The latter experiences the largest frequency shift of all modes in the anharmonic calculation (+843 $cm^{-1}$). As can be seen, this mode resembles an inversion vibration of the N–H bond, which is known to be very anharmonic. Hence, this large anharmonic correction confirms the validity of the anharmonic calculations for the presented analysis.

*3.2.2. Transition dipole moment orientation*

The direction of the transition dipole moment (TDM) in the molecular frame is an important indicator for the electronic nature of the excited state. For a planar molecule its orientations with respect to the inertial $a$ and $b$-axes are defined via the angle $\theta$, which is the angle of the transition moment vector with the molecule fixed $a$-axis:

$$\mu_a = \mu\cos\theta \quad \text{and} \quad \mu_b = \mu\sin\theta$$

The squares of the projections onto the inertial axes are directly proportional to the experimentally observed contribution to the band type in the electronic absorption spectrum. The SCS-CC2 calculations yield comparably small values of $\theta$ for the $S_1$ state (9°) as observed in experiment, while the value obtained for the $S_2$ state is much larger (65°). Thus, the calculations confirm the experimental finding that the TDM orientation of the lowest electronically excited state is mainly directed along the $a$-axis. The transition to the second excited singlet state is predicted to an $ab$-hybrid, with predominantly $b$-type.

In a previous publication we have shown, that the excitations to the $S_1$ and $S_2$ states are heavily mixed and the second excited singlet state is accompanied by a considerable charge migration from the indolic NH group to the cyano group [15]. The vibronic bands at 349 and 884 $cm^{-1}$ have a considerably larger transition dipole moment angle $\theta$ than the origin band. Since the origin of the next excited singlet state $S_2$ is expected to be adiabatically more than 3000 $cm^{-1}$ higher in energy [15], the only mechanism which can give rise to such a strong change in the TDM is vibronic coupling of these modes to the perturbing $S_2$ state.

## 4. Conclusions

The vibrational bands at 349 and 884 $cm^{-1}$ above the electronic origin were recorded at rotational resolution and analyzed using an asymmetric rotor Hamiltonian by means of an evolutionary strategy approach. Comparison to anharmonic corrections calculated at the MP2 (6-31G(d,p)) level of theory to the experimentally determined values allowed an assignment of the observed vibrations. This assignment is not only based on the corrected frequencies but accounts for vibrationally induced changes to the excited state geometry as well. Both changes in the rotational constants and the planarity of the molecule are made use of.

The orientation of the TDM vector deviates for both vibrational bands significantly from the value reported for the vibrationless origin [15]. As the change in the TDM orientation is more pronounced for the band at 349 $cm^{-1}$ than for the band at 884 $cm^{-1}$ (+29° compared to +19°), mode-selective coupling to an electronic state lying higher in energy is to be expected. A Herzberg–Teller analysis [32] would be required to explain the observed effects as it has been done before in our group for both indole [5] and tryptamine [33]. The respective analysis is being prepared to answer this question.

## Acknowledgement

This work was financially supported by the Deutsche Forschungsgemeinschaft SCHM1043/12-1.

## Appendix A. Supplementary material

Supplementary data associated with this article can be found, in the online version, at http://dx.doi.org/10.1016/j.molstruc.2012.11.049.

## References


[1] J.R. Platt, J. Chem. Phys. 17 (1949) 484–495.
[2] P.R. Callis, J. Chem. Phys. 95 (1991) 4230.
[3] P.R. Callis, in: J. Lakowicz (Ed.), Topics in Fluorescence Spectroscopy, vol. 5, Plenum Press, New York, 1977, pp. 1–42.
[4] D.M. Sammeth, S. Yan, L.H. Spangler, P.R. Callis, J. Phys. Chem. 94 (1990) 7340.
[5] C. Brand, J. Küpper, D.W. Pratt, W.L. Meerts, D. Krügler, J. Tatchen, M. Schmitt, Phys. Chem. Chem. Phys. 12 (2010) 4968–4997.
[6] J. Küpper, D.W. Pratt, W.L. Meerts, C. Brand, J. Tatchen, M. Schmitt, Phys. Chem. Chem. Phys. 12 (2010) 4980–4988.
[7] G. Berden, W.L. Meerts, E. Jalviste, J. Chem. Phys. 103 (1995) 9596–9606.
[8] B. Albinsson, B. Nordén, J. Phys. Chem. 96 (1992) 6204.
[9] C. Brand, O. Oeltermann, D.W. Pratt, R. Weinkauf, W.L. Meerts, W. van der Zande, K. Kleinermanns, M. Schmitt, J. Chem. Phys. 133 (2010). 024303-1–024303-11.
[10] O. Oeltermann, C. Brand, W.L. Meerts, J. Tatchen, M. Schmitt, J. Mol. Struct. 933 (2011) 2–8.
[11] K.W. Short, P.R. Callis, Chem. Phys. 283 (2002) 269.
[12] B. Fender, P.R. Callis, Chem. Phys. Letters 262 (1996) 343–348.
[13] A.A. Rehms, P.R. Callis, Chem. Phys. Letters 140 (1987) 83.
[14] Y. Huang, M. Sulkes, Chem. Phys. Letters 254 (1996) 242–248.
[15] O. Oeltermann, C. Brand, B. Engels, J. Tatchen, M. Schmitt, Phys. Chem. Chem. Phys. 114 (2012) 10266–10270.
[16] M. Schmitt, J. Küpper, D. Spangenberg, A. Westphal, Chem. Phys. 254 (2000) 349–361.
[17] S. Gerstenkorn, P. Luc, Atlas du spectre d'absorption de la molécule d'iode, CNRS, Paris, 1982.
[18] R. Ahlrichs, M. Bär, M. Häser, H. Horn, C. Kölmel, Chem. Phys. Letters 162 (1989) 165–169.
[19] J.T.H. Dunning, J. Chem. Phys. 90 (1989) 1007–1023.
[20] C. Hättig, F. Weigend, J. Chem. Phys. 113 (2000) 5154–5161.
[21] C. Hättig, A. Köhn, J. Chem. Phys. 117 (2002) 6939–6951.
[22] C. Hättig, J. Chem. Phys. 118 (2002) 7751–7761.
[23] A. Hellweg, S. Grün, C. Hättig, Phys. Chem. Chem. Phys. 10 (2008) 1159–1169.
[24] TURBOMOLE V6.1 2009, a development of University of Karlsruhe and Forschungszentrum Karlsruhe GmbH, 1989–2007, TURBOMOLE GmbH, since 2007. <http://www.turbomole.com>.
[25] V. Barone, J. Chem. Phys. 122 (2005). 014108-1–014108-10.
[26] M.J. Frisch, G.W. Trucks, H.B. Schlegel, G.E. Scuseria, M.A. Robb, J.R. Cheeseman, J.A. Montgomery Jr., T. Vreven, K.N. Kudin, J.C. Burant, J.M. Millam, S.S. Iyengar, J. Tomasi, V. Barone, B. Mennucci, M. Cossi, G. Scalmani, N. Rega, G.A. Petersson, H. Nakatsuji, M. Hada, M. Ehara, K. Toyota, R. Fukuda, J. Hasegawa, M. Ishida, T. Nakajima, Y. Honda, O. Kitao, H. Nakai, M. Klene, X. Li, J.E. Knox, H.P. Hratchian, J.B. Cross, C. Adamo, J. Jaramillo, R. Gomperts, R.E. Stratmann, O. Yazyev, A.J. Austin, R. Cammi, C. Pomelli, J.W. Ochterski, P.Y. Ayala, K. Morokuma, G.A. Voth, P. Salvador, J.J. Dannenberg, V.G. Zakrzewski, S. Dapprich, A.D. Daniels, M.C. Strain, O. Farkas, D.K. Malick, A.D. Rabuck, K. Raghavachari, J.B. Foresman, J.V. Ortiz, Q. Cui, A.G. Baboul, S. Clifford, J. Cioslowski, B.B. Stefanov, G. Liu, A. Liashenko, P. Piskorz, I. Komaromi, R.L. Martin, D.J. Fox, T. Keith, M.A. Al-Laham, C.Y. Peng, A. Nanayakkara, M. Challacombe, P.M.W. Gill, B. Johnson, W. Chen, M.W. Wong, C. Gonzalez, J.A. Pople, Gaussian 03, revision a.1 Gaussian, Inc., Pittsburgh, PA, 2003.
[27] A. Ostermeier, A. Gawelczyk, N. Hansen, Lecture Notes in Computer Science: Parallel Problem Solving from Nature (PPSN III), Springer, 1994. pp. 189–198.
[28] N. Hansen, A. Ostermeier, Evol. Comput. 9 (2) (2001) 159–195.
[29] W.L. Meerts, M. Schmitt, Int. Rev. Phys. Chem. 25 (2006) 353–406.
[30] O.M. Shir, T. Bäck, Proceedings of the Genetic and Evolutionary Computation Conference, ACM Press, London, 2007. pp. 713–721.
[31] W. Gordy, R.L. Cook, Microwave Molecular Spectra, third ed., Wiley, New York, 1984.
[32] G. Herzberg, Molecular Spectra and Molecular Structure, III. Electronic Spectra and Electronic Structure of Polyatomic Molecules, van Nostrand Reinhold Company, New York, 1966.
[33] M. Böhm, J. Tatchen, D. Krügler, K. Kleinermanns, M.G.D. Nix, T.A. LeGreve, T.S. Zwier, M. Schmitt, J. Phys. Chem. A 113 (2009) 2456–2466.